PROCEEDINGS, 43rd Workshop on Geothermal Reservoir Engineering
Stanford University, Stanford, California, February 12-14, 2018
SGP-TR-213

Study on Seismic Events Induced by Loss of Fault Confinement due to Rock Temperature Decrease in EGS Reservoirs

Zoheir Khademian, Masami Nakagawa, and Ryan Garvey

1500 Illinois St., Mining Department # 227, Golden CO USA 80401

zoheirkhademian@gmail.com

Keywords: Rock temperature, induced seismic event, radiated seismic energy, fault brittleness

ABSTRACT

Heat is extracted from geothermal reservoirs and the altered thermal conditions of rock perturb *in-situ* stresses and may induce slip (shear displacement discontinuity) on pre-existing faults. Noticeable seismic events may arise as a consequence of the thermally induced slip. This paper focuses on impacts of cooling on the loss of fault confinement and triggering a rupture (seismic slip). We simulate a preexisting, strike-slip fault and calibrate the dynamic rupture modeling by checking results against an analytical solution. The calibrated model is then used for simulating thermally induced rupture along faults with different initial stresses. We explore effects of cooling rock on triggering a seismic slip along the fault while the temperature of surrounding rock continuously decreases from 400 ºC until slip occurs. We study fault models with which initial shear stresses on the fault are six different fractions of the fault peak shear strength. An energy-based numerical methodology, previously developed and verified by the authors, is employed to simulate the intensity of rupture through calculating radiated seismic energy from each fault model. Results show that the fault with initial shear stresses closer to the fault shear strength is activated by smaller disturbances in rock temperature and generates rupture with higher radiated seismic energy. The induced rupture generates less radiated seismic energy for faults that are not close to the brink of failure and thus require a higher thermal drawdown before activation.

1. INTRODUCTION

Enhanced Geothermal Systems (EGS) are human-made reservoirs characterized by the use of hydraulic fracturing to increase flow rate between injection and production wells in high temperature, low permeability rocks. One of the challenges in developing the EGS is dealing with seismic events that may arise as a consequence of the induced slip and can sometimes be felt at the surface. Besides microseismicity noted during the stimulation process, long-term production can also cause noticeable seismic events away from the injection wells (Majer et al., 2007). Ellsworth (2013) and Khademian et al. (2017) showed that induced seismicity along preexisting discontinuities occurs when the mechanical equilibrium underground is disturbed by engineering activities in the fractured ground. The exploitation of geothermal energy involves changes in mechanical equilibrium underground mostly by altering temperature and pore pressure of rock formations. The process of regaining the mechanical equilibrium mostly accompanies slip along preexisting discontinuities within the affected zone. The induced slip can be unstable, leading to a rupture (seismic slip) with a significant release of seismic energy; or the induced slip can be stable, causing creep (aseismic slip).

This paper excludes possible other triggers of seismicity, e.g. pore pressure alteration, in EGS and mechanistically studies the role of reservoir temperature decrease in inducing slip and its stability. We construct a strike-slip fault model in the Universal Distinct Element Code (UDEC) and calibrate the mesh geometry and loading conditions for the dynamic rupture simulation by checking the resulting rupture length, slip magnitude, and seismic energy against analytic solutions. Then, we simulate the rock volume contraction imposed by cooling the rock around the fault and study its role in triggering a slip. Stability of the induced slip is then investigated by a methodology previously developed by the authors (Z. Khademian et al. 2016; Khademian & Nakagawa, in press) in which radiated seismic energy is estimated by calculating the difference between the energy available for slip and the energy consumed during slip.

2. METHODOLOGY

The gravitational and tectonic loading are the major external forces that generate interseismic, steady deformation, of rockmass which results in an accumulation of strain energy (U_i) prior to the slip. The active external forces can also produce the external work (W) through continued deformations as the slip occurs. By altering the temperature of rock formations, the exploitation of geothermal energy reduces the rock thermal energy (Q_c) within the influenced zone, thereby disturbing the mechanical equilibrium underground. Note that accounting for term Q_c is the modification that this paper makes to the methodology previously developed by the authors (Khademian et al. 2017). Regaining the equilibrium requires a release of the accumulated strain energy mostly through a slip along a preexisting fault. Slip does not lead to a complete exhaustion of the stored energy and some residual strain energy (U_r) will remain in the fault system (Brune 1970). The slip is accompanied by dissipative energy terms in the form of plastic work (W_p) and radiated seismic energy (W_k). During an aseismic slip, the partial release of the strain energy is fully consumed by the plastic work W_p generated by the friction along the activated fault and thus near-zero W_k is radiated. However, in the course of a rupture, the strain energy release is not completely exhausted by W_p and is radiated in the form of W_k (Salamon 1970; Rice 1983). A static energy balance can summarize the transfer of energy, as shown in Equation 1 where the left side shows the available energy before slip and right side represents the post-rupture state of energy.

$$W + U_i + Q_c = W_p + U_r + W_k \quad (1)$$

Note that mechanical work done by injection pressure can also play a role in triggering slip (Khademian & Nakagawa, in press), but here we ignore effects of this energy component and exclusively focus on the cooling impact on triggering slip. Rearranging the energy balance, we can calculate the seismic energy radiated from a slip as

$$W_k = W + \Delta U + Q_c - W_p \quad (2)$$

where ΔU is the release of the strain energy during the slip. We can numerically calculate each energy term in Equation 2 and obtain the radiated seismic energy during a rupture. The mechanical damping of the Distinct Element Method (DEM) scheme in UDEC also allows the dynamic calculation of the seismic energy. In order to reach a solution of static equilibrium for each dynamic system, the quasi-static approach in UDEC extracts a fraction of the kinetic energy of the system at each time step and records this cumulative term as damped work (W_D). The remaining kinetic energy (U_k) is also recorded as a non-cumulative term. U_k is near zero as the model reaches equilibrium and is high during the simulation of a dynamic response (Poeck et al., 2016). The seismic energy calculation based on the kinetic terms in the system is governed by Equation (3) (ITASCA, 2016).

$$W_k = U_k + W_D \quad (3)$$

Our previous findings (Khademian et al. 2016) show that the seismic energy calculated by the dynamic approach of Equation 3 is in agreement with the results of Equation 2 and those of the analytical solutions provided by Duvall and Stephenson (1965), Salamon (1984), and Cook (1966). Depending on the capability of the numerical method, either of these two equations can be used to estimate radiated seismic energy. This paper first simulates a fault activation and calibrates the model mesh geometry and fault modeling approach by comparing the results with analytical solutions given by (Ryder 1988). We then further develop the methodology to study seismicity induced by thermal drawdown.

3. MODELING DYNAMIC RUPTURE ON STRIKE-SLIP FAULT

Modeling rupture dynamics along a fault requires a careful study of the model mesh geometry and loading conditions. Loading conditions influence normal and shear load distributions over a fault and thus control the rupture length and the seismic energy magnitude (Madariaga et al. 1998). Mesh geometry affects the shear slip localization and the location of rupture initiation (Khademian et al. 2017). Using analytical functions for rupture calculations provided by Ryder (1988), we optimized the mesh geometry and defined an effective loading condition through a trial and error process. Here, we only show results of the calibration process through comparing final numerical and analytical values.

Ryder (1988) analyzed five families of possible shear stress distributions along a fault characterized with an abrupt stress drop and derived the resulting rupture length, slip profile, seismic moment, and seismic energy in each case. We numerically constructed a fault and activated it by various loading conditions: applying force to the outer boundary of the model, applying single force couple at the fault center, and applying both uniformly distributed and non-uniformly distributed force couples. A frictional behavior with an abrupt stress drop is assigned to the fault by the Mohr-Coulomb constitutive law with initial and residual friction coefficients of 0.6 and 0.49, respectively. Figure 1 indicates the frictional behavior assigned to each element along the fault. Assuming a 90 MPa normal stress acting on the fault, initial and residual fault strengths equal 54 and 44 MPa, respectively.

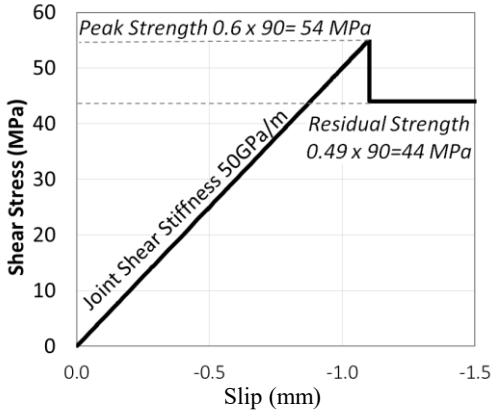

Figure 1. Frictional properties assigned to each element along the fault for simulating the abrupt stress drop following Ryder (1988).

The non-uniformly distributed force couples with the pattern shown in Figure 2 were found to produce the 2-D symmetrical shear stress profile, one of the five families of the shear stress distribution developed by Ryder (1988). The effective mesh geometry was also found to follow a 1:40 mesh size to rupture length ratio. The non-uniformly distributed force couples gradually increase from zero to 17 MN, following the pattern shown in Figure 2. The incremental quasi-static loading develops U_i and remains constant once rupture initiates, but the rupture self-propagates as ΔU and W are enough to drive the rupture progression. Once ΔU is exhausted and W can no longer

overcome the shear strength of the neighboring segments, the rupture is arrested. Note that following assumptions made by Ryder (1988), the matrix is assumed elastic and W_p excludes the fracturing energy that is necessary to create new surfaces branching off from the fault.

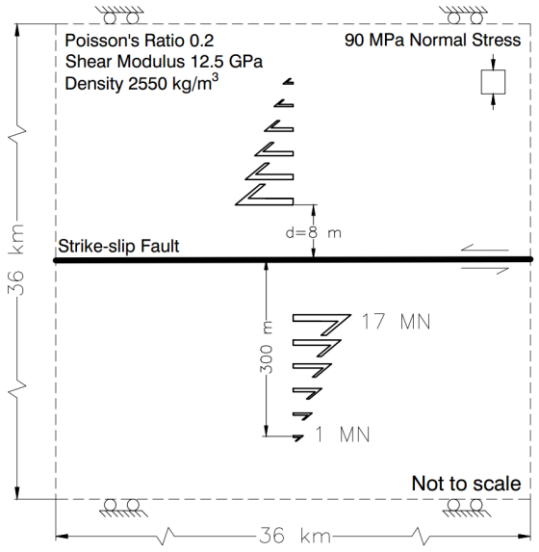

Figure 2. The 2-D numerical model geometry and initial conditions on the plan view of the strike-slip fault

Figure 3a shows the 2D symmetrical stress profile obtained by UDEC and analytical functions based on the Excess Shear Stress (ESS) concept. ESS is the difference between the fault shear stress and dynamic strength on each element. In Figure 3a, dots are the ESS values recorded along the simulated fault in UDEC and the solid line is the driving ESS profile obtained by Ryder (1988). Figure 3b shows the slip at points along the rupture plane from the numerical results and Ryder's calculations.

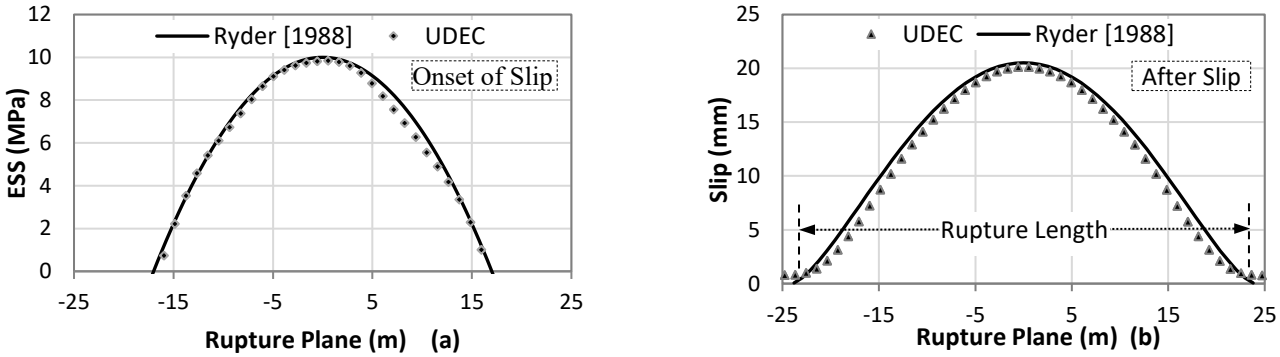

Figure 3. a) Comparison between analytical and numerical solutions for driving ESS profile; c) Analytical and numerical solutions for slip along a brittle fault

Table 2 shows the comparison between numerical results and analytical solutions for rupture length, average ride, and seismic energy. The seismic energy calculated within UDEC is 1.8 MJ as compared to the analytical result of 1.9 MJ for an error of 4%. There are errors of 2% and 5% for rupture length and average slip values, respectively. Because the ESS profile mainly drives the resulting source parameters, the errors mostly originate from relatively insignificant mismatching between numerical and analytical ESS profiles in Figure 3a. The agreement between results indicates that the loading condition and mesh geometry are calibrated. This allows further studying the propagation and arrest of a rupture induced by thermal triggers.

Table 2. Comparison between rupture characteristics obtained by UDEC and Ryder (1988)

Method	Peak ESS	Mean ESS	Mean Slip	Rupture Length	Seismic Energy
	MPa	MPa	mm	m	MJ
Ryder's method	10.0	6.5	12.9	44.2	1.9
UDEC results	10.0	6.6	12.3	45.1	1.8
Error		2%	5%	2%	4%

4. MODELING THERMALLY INDUCED SLIP

Long-term injection of cold fluid gradually cools rock in a geothermal reservoir. The reduced rock temperature can re-distribute in-situ stresses around a preexisting fault, resulting in a slip. Dependent on the rock thermal expansion coefficient, temperature decrease reduces the volume of the rock within the affected zone. Two mechanisms mainly govern thermally induced slip events. Rock shrinkage in the vicinity of the fault can reduce the normal stress acting on the fault, degrade the initial strength of the fault, and ultimately induce the slip. Asymmetric cooling of rocks can also induce shear stresses on preexisting discontinuities, overcome the initial strength of the fault, and trigger the slip. However, this paper simulates a slip triggered by the reduction in the fault initial strength due to the loss of the fault confinement caused by rock shrinkage. In this mechanism, Q_c triggers slip by reducing the rock capacity for storing U_i through reducing the normal stress on the fault. Following the same process, Q_c also reduces the rock capacity for storing U_r after slip is initiated. We study this concept through modeling faults with different initial shear stresses.

Adopting the calibrated fault model described in the previous section, we set an initial temperature of 400 ºC to the entire model and then reduce the temperature of the rock around the fault by imposing a cooling source over a centered 200 m length of the fault. The cooling source reduces the rock temperature gradually, a simplified analogy for the gradual thermal drawdown in a geothermal setting. As the simulation continues, more heat is extracted from the rock and the affected zone grows. Here, we simulate six fault activation scenarios where initial shear stresses on the fault are various fractions of the initial fault strength (54 MPa). We simulate faults loaded to 99%, 98%, 97%, 96%, 95%, and 94% of their initial strength and then start reducing the temperature. Note that temperature reduction does not change the initial shear stresses but decreases the fault strength. Figure 4 shows the shear stress versus slip curves for each scenario, recorded at the center of the activated fault. The elastic modulus of the rock surrounding the fault is assumed 30 GPa.

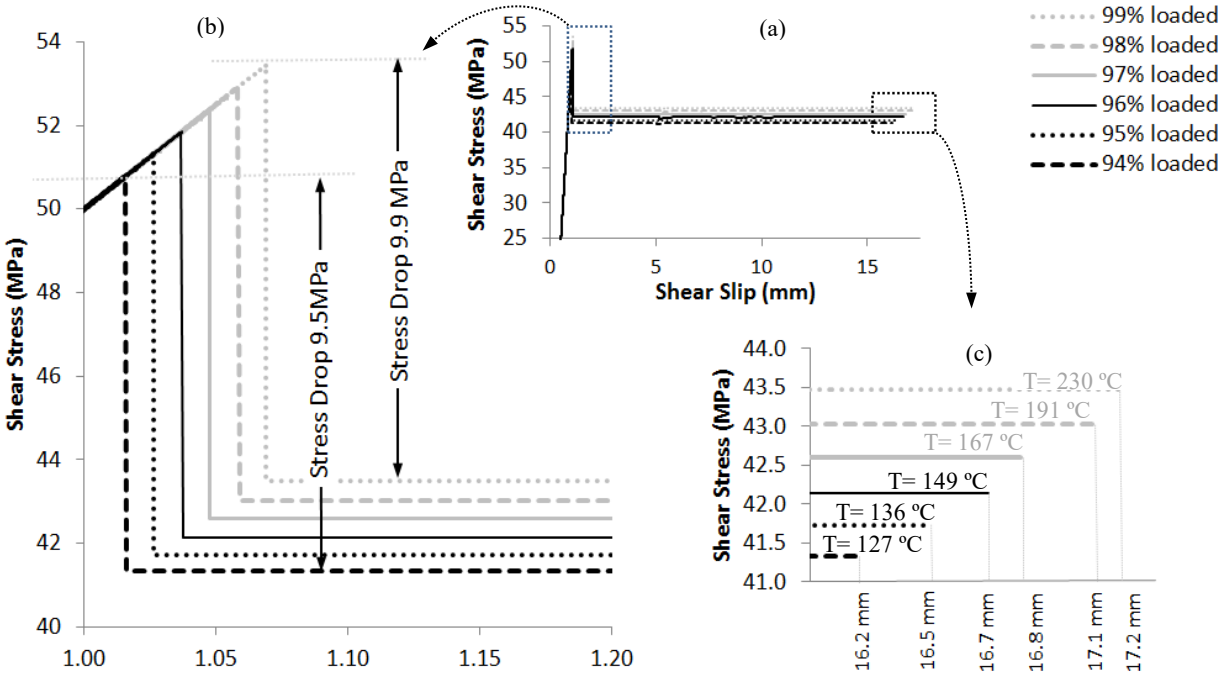

Figure 4. Modeling results of the fault activation induced by the rock volume contraction imposed by cooling the rock.

Figure 4a provides the overall trend of the shear stress and displacement along the fault while more details on the stress drop and slip are given by parts (b) and (c), respectively. Figure 4c also shows the rock temperatures at the center of the fault at the onset of slip. The thermally induced rock shrinkage reduces the normal stress on the fault, degrading the strength of the fault, thereby inducing a slip. The highest stress drop of 9.9 MPa in Figure 4b is associated with the fault loaded to 99% of its initial shear strength of 54 MPa. The 94% loaded fault introduces the lowest stress drop of 9.5 MPa. This is because the stress drop is a function of the normal stress on the fault and the normal stress depends on the level of temperature reduction. The difference in slip temperatures shown in Figure 4c explains this variation in the stress drop in Figure 4a. The 99% loaded fault demands the lowest temperature decrease from 400 to 230 ºC for activating the fault while the rock temperature needs to be as low as 127 ºC before slip is initiated along the 94% loaded fault. The former case requires less reduction in the normal stress before the slip initiation while the latter needs a higher loss of confinement.

The stress drop variations are also the underlying cause of the trend of the slip values in Figure 4c. The fault stress drop dictates the magnitude of the energy available for slip ($W + \Delta U$) such that the 99% loaded fault accommodates the highest available energy (Khademian et al. 2017). Higher available energy further dislocates fault planes before slip is terminated, resulting in the increasing trend in Figure 4c as the fault's shear stresses and therefore stress drops are increased. Based on Equation 2, higher available energy also further increases the radiated seismic energy from a fault slip, meaning under constant frictional properties, highly loaded faults store higher strain energy and accordingly generate higher magnitude events once rupture is triggered. This is confirmed by Figure 5 that indicates the increasing trend of the radiated seismic energy as a function of the fault loading condition.

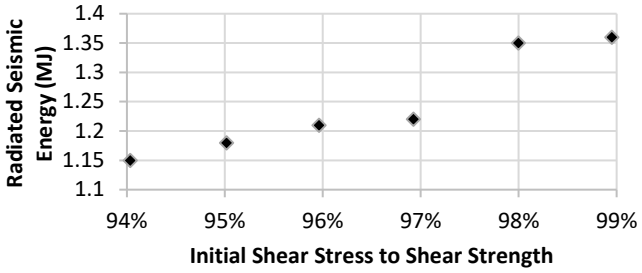

Figure 5. Variations between the radiated seismic energy and the fault initial loading conditions

Figure 5 shows that the level of instability or intensity of a rupture induced by temperature disturbance depends on the initial stresses on the fault. Less critically loaded faults, e.g. with initial stresses that are 94% of the peak strength, generate ruptures with a radiated seismic energy magnitude of 1.15 MJ. As the initial shear stresses approach the peak strength of the fault (54 MPa), more critically loaded faults are simulated and the magnitude of radiated seismic energy increases to 1.36 MJ.

5. DISCUSSION AND FUTURE RESEARCH

We simulate thermally induced slip and discuss the loss of fault confinement as one of the possible contributions of rock temperature disturbance to triggering seismic events in EGS projects. We show the fault that is critically loaded and is close to the brink of slip can be activated by the smallest reduction in the rock temperature. Otherwise, the more thermal drawdown is required for sufficiently reducing the fault strength and initiating slip. More critically loaded faults are prone to generate higher stress drop, higher slip, and finally higher-magnitude seismic events. Figure 5 shows that slip on all faults that are simulated in this paper generate some level of radiated seismic energy. That is, we do not show examples of stable slip where available energy is fully consumed by W_P and near-zero W_k is radiated. However, stable slip should be studied for better understanding unstable events.

Khademian et al. (2017) numerically showed that loading system stiffness and slip-weakening characteristics of the fault play significant roles in the slip instability. Stable slip along a fault is possible once the fault behaves in a slip-weakening manner and the loading system is stiff enough. The rock elastic modulus controls the loading system stiffness that is inversely related to the magnitude of radiated energy. The slip-weakening characteristics are mainly driven by the characteristic distance (D_c), which is the slip distance required for the initial shear stress on the fault to reach the residual state. Khademian et al. (2017) argued that lower D_c leads to higher energy radiation. As a result, slip events in Figure 5 are unstable because an abrupt stress drop with zero D_c, simulated by the frictional characteristics in Figure 1, guarantees instability.

Using field or laboratory observations for more realistically estimating D_c and the rock elastic modulus can help study both stable and unstable slip events in EGS because any temperature-dependent alteration in D_c or loading system stiffness affects the slip instability. Existing experimental studies on different types of granite, which are the most common lithologies hosting EGS projects, suggest that rock temperature alters elastic modulus of the rock (Figure 6a) and slip-weakening behavior of adjacent faults (Figure 6b).

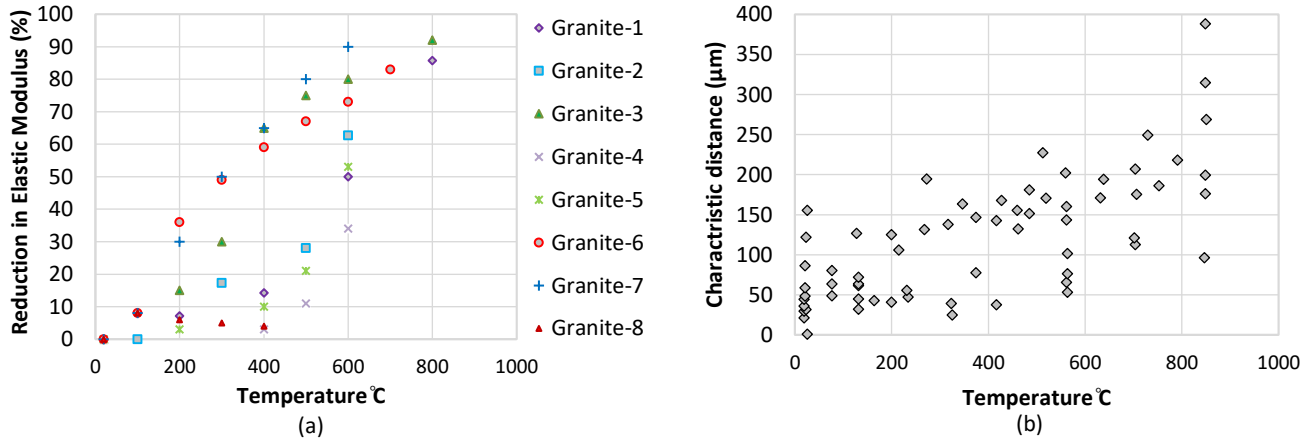

Figure 6. (a) Effects of temperature on elastic moduli of different types of granite; Granite 1(Chen et al. 2012); Granite 2 (Takarli & Prince-Agbodjan 2008); Granite 3 (Dwivedi et al. 2008); Granite 4, 5, 6, 7, and 8 (Heuze 1983) (b) Changing the characteristic distance of a fault as a function of temperature for granite (Chester 1994; Lockner et al. 1986; Morrow et al. 2000)

Evidence provided by Figure 6a suggests that a reduction in temperature can increase the elastic modulus of granite. Figure 6b shows the influence of temperature on D_c, suggesting that cooling rock around a fault reduces the characteristic distance on the fault. Future

studies are required to explore the role of temperature-dependent elastic modulus and characteristic distance in thermally induced slip and its stability.

REFERENCES

Brune, J.N., 1970. Tectonic stress and the spectra of seismic shear waves from earthquakes. *Journal of Geophysical Research*, 75(26), pp.4997–5009. Available at: http://doi.wiley.com/10.1029/JB075i026p04997 [Accessed August 2, 2017].

Chen, Y.-L. et al., 2012. Experimental study on the influence of temperature on the mechanical properties of granite under uni-axial compression and fatigue loading. *International Journal of Rock Mechanics and Mining Sciences*, 56, pp.62–66.

Chester, F.M., 1994. Effects of temperature on friction: Constitutive equations and experiments with quartz gouge. *Journal of Geophysical Research*, 99(B4), p.7247. Available at: http://doi.wiley.com/10.1029/93JB03110 [Accessed February 2, 2018].

Dwivedi, R.D. et al., 2008. Thermo-mechanical properties of Indian and other granites. *International Journal of Rock Mechanics and Mining Sciences*, 45(3), pp.303–315. Available at: https://www.sciencedirect.com/science/article/pii/S1365160907000822 [Accessed February 2, 2018].

Ellsworth, W.L., 2013. Injection-Induced Earthquakes. *Science*, 341(6142). Available at: http://science.sciencemag.org/content/sci/341/6142/1225942.full.pdf [Accessed October 30, 2017].

Heuze, F.E., 1983. High-temperature mechanical, physical and Thermal properties of granitic rocks— A review. *International Journal of Rock Mechanics and Mining Sciences & Geomechanics Abstracts*, 20(1), pp.3–10. Available at: https://www.sciencedirect.com/science/article/pii/0148906283916091 [Accessed February 2, 2018].

Hosseini, A., 2014. Stabilization and Improvement of Collapsible Soils, Using Electrokinetics & Nanomaterials and Assessment Its Strength Parameters by Unsaturated Oedometer. Thesis, Sharif University of Technology DOI: 10.13140/RG.2.2.23851.95526/1

Itasca, 2016. Background - The 2D Distinct Element Method, UDEC Manual.

Khademian, Z. et al., 2017. Role of Fluid Injection Pressure in Inducing Seismicity. In *Proceedings of the 42nd Workshop on Geothermal Reservoir Engineering*. p. 10.

Khademian, Z. et al., 2016. Studies of seismicity generated by unstable failures around circular excavations. In *50th US Rock Mechanics / Geomechanics Symposium 2016*.

Khademian, Z. & Nakagawa, M., *Modeling Injection-Induced Seismicity by Energy Calculation*, in Press. Journal of Natural Gas Science and Engineering

Khademian, Z. & Nakagawa, M., Modeling Rupture Propagation based on Seismic Energy Calculations. *Submitted to Journal Geophysical Research*.

Khosravi, A., Rahimi, M., Gheibi, A., & Mahdi Shahrabi, M. ,2017. Impact of Plastic Compression on the Small Strain Shear Modulus of Unsaturated Silts. *International Journal of Geomechanics*, 18(2), 04017138.

Lockner, D.A., Summers, R. & Byerlee, J.D., 1986. Effects of temperature and sliding rate on frictional strength of granite. *Pure and Applied Geophysics PAGEOPH*, 124(3), pp.445–469. Available at: http://link.springer.com/10.1007/BF00877211 [Accessed February 2, 2018].

Madariaga, R., Olsen, K. & Archuleta, R., 1998. Modeling Dynamic Rupture in a 3D Earthquake Fault Model. *Bulletin of the Seismological Society of America*, 88(5), pp.1182–1197. Available at: https://gsw.silverchair-cdn.com/gsw/Content_public/Journal/bssa/88/5/0037110688050007/3/BSSA0880051182.pdf?Expires=1515617471&Signature=FDu4vOj~WGr2TS38OL7~dU~26-0d~xLmAq9eNrfJv6zMOpUB5naB5fMSPK5M8OLDAM3W1OR80TmurCk1Vrf3CnEO-Lxu1Gep~5qF4h7iT2vAk2QZJZGqPak [Accessed January 9, 2018].

Morrow, C.A., Moore, D.E. & Lockner, D.A., 2000. The effect of mineral bond strength and adsorbed water on fault gouge frictional strength. *Geophysical Research Letters*, 27(6), pp.815–818. Available at: http://doi.wiley.com/10.1029/1999GL008401 [Accessed February 2, 2018].

Poeck, E. et al., 2016. Modeling unstable rock failures in underground excavations. In *Rock Mechanics and Rock Engineering: From the Past to the Future*. Taylor & Francis Group, 6000 Broken Sound Parkway NW, Suite 300, Boca Raton, FL 33487-2742: CRC Press, pp. 505–509. Available at: http://www.crcnetbase.com/doi/10.1201/9781315388502-86 [Accessed March 15, 2017].

Rice, J.R., 1983. Constitutive relations for fault slip and earthquake instabilities. *Pure and Applied Geophysics PAGEOPH*, 121(3), pp.443–475. Available at: http://link.springer.com/10.1007/BF02590151 [Accessed March 15, 2017].

Ryder, J. a., 1988. Excess shear stress in the assessment of geologically hazardous situations. *J. South African Inst. Mining Metallurgy*, 88(1), pp.27–39.

Salamon, M.D.G., 1984. Energy considerations in rock mechanics: fundamental results. , 84(8), pp.233–246. Available at: https://www.saimm.co.za/Journal/v084n08p233.pdf [Accessed March 15, 2017].

Salamon, M.D.G., 1970. Stability, instability and design of pillar workings. *International Journal of Rock Mechanics and Mining Sciences and*, 7(6), pp.613–631.

Takarli, M. & Prince-Agbodjan, W., 2008. Temperature Effects on Physical Properties and Mechanical Behavior of Granite: Experimental Investigation of Material Damage. *Journal of ASTM International*, 5(3).